

# Seismic Electric Signals and $1/f$ “noise” in natural time

P. A. Varotsos,<sup>1,2,\*</sup> N. V. Sarlis,<sup>1</sup> and E. S. Skordas<sup>1,2</sup>

<sup>1</sup>*Solid State Section, Physics Department, University of Athens,  
Panepistimiopolis, Zografos 157 84, Athens, Greece*

<sup>2</sup>*Solid Earth Physics Institute, Physics Department,  
University of Athens, Panepistimiopolis, Zografos 157 84, Athens, Greece*

By making use of the concept of natural time, a simple model is proposed which exhibits the  $1/f^a$  behavior with  $a$  close to unity. The properties of the model are compared to those of the Seismic Electric Signals (SES) activities that have been found to obey the ubiquitous  $1/f^a$  behavior with  $a \approx 1$ . This comparison, which is made by using the most recent SES data, reveals certain similarities, but the following important difference is found: The model suggests that the entropy  $S_-$  under time reversal becomes larger compared to the entropy  $S$  in forward time, thus disagreeing with the experimental SES results which show that  $S$  may be either smaller or larger than  $S_-$ . This might be due to the fact that SES activities exhibit *critical* dynamics, while the model cannot capture all the characteristics of such dynamics.

PACS numbers: 05.40.-a, 05.45.Tp, 91.30.Dk, 89.75.-k

## I. INTRODUCTION

Among the different features that characterize complex physical systems, the most ubiquitous is the presence of  $1/f^a$  noise in fluctuating physical variables[1]. This means that the Fourier power spectrum  $S(f)$  of fluctuations scales with frequency  $f$  as  $S(f) \sim 1/f^a$ . The power-law behavior often persists over several orders of magnitude with cutoffs present at both high and low frequencies. Typical values of the exponent  $a$  approximately range between 0.8 and 4 (e.g., see Ref.[2] and references therein), but in a loose terminology all these systems are said to exhibit  $1/f$  “noise”. Such a “noise” is found in a large variety of systems, e.g., condensed matter systems(e.g. [3]), freeway traffic[4, 5, 6], granular flow[7], DNA sequence[8], heartbeat[9], ionic current fluctuations in membrane channels[10], river discharge[11], the number of stocks traded daily[12], chaotic quantum systems[13, 14, 15, 16], the light of quasars[17], human cognition[18] and coordination[19], burst errors in communication systems[20], electrical measurements[21], the electric noise in carbon nanotubes[22] and in nanoparticle films[23], the occurrence of earthquakes[24] etc. In some of these systems, the exponent  $a$  was reported to be very close to 1, but good quality data supporting such a value exist in a few of them[3]. As a first example we refer to the voltage fluctuations when current flows through a resistor[25]. As a second example we mention the case of Seismic Electric Signals (SES) activities which are transient low frequency ( $\leq 1$ Hz) signals observed before earthquakes [26, 27, 28, 29, 30, 31, 32, 33, 34], since they are emitted when the stress in the focal region reaches a *critical* value before the failure[35, 36]. These electric signals, for strong earthquakes with magnitude 6.5 or larger, are also accompanied by detectable magnetic

field variations[37, 38, 39]. Actually, the analysis of the original time series of the SES activities have been shown to obey a  $1/f$ -behavior[40, 41].

The  $1/f^a$  behavior has been well understood on the basis of dynamic scaling observed at *equilibrium* critical points where the power-law correlations in time stem from the infinite-range correlations in space (see Ref.[2] and references therein). Most of the observations mentioned above, however, refer to *nonequilibrium* phenomena for which -despite some challenging theoretical attempts[42, 43, 44, 45]- possible *generic* mechanisms leading to scale invariant fluctuations have not yet been identified. In other words, despite its ubiquity, there is no yet universal explanation about the phenomenon of the  $1/f^a$  behavior. Opinions have been expressed (e.g., see Ref.[13]) that it does not arise as a consequence of particular physical interactions, but it is a generic manifestation of complex systems.

It has been recently shown[40, 49, 50, 51, 52, 53, 54, 55, 56, 57, 58, 59, 60] that novel dynamic features hidden behind the time series of complex systems can emerge if we analyze them in terms of a newly introduced time domain, termed natural time  $\chi$  (see below). It seems that this analysis enables the study of the dynamic evolution of a complex system and identifies when the system enters a critical stage. Natural time domain is optimal[61] for enhancing the signal’s localization in the time frequency space, which conforms to the desire to reduce uncertainty and extract signal information as much as possible. In a time series comprising  $N$  events, the *natural time*  $\chi_k = k/N$  serves as an index[40, 49, 50] for the occurrence of the  $k$ -th event. The evolution of the pair  $(\chi_k, Q_k)$  is studied[36, 40, 49, 50, 51, 52, 53, 54, 55, 56, 58, 59], where  $Q_k$  denotes a quantity proportional to the energy released in the  $k$ -th event. For example, for dichotomous signals, which is frequently the case of SES activities,  $Q_k$  stands for the duration of the  $k$ -th pulse. The normalized power spectrum  $\Pi(\omega) \equiv |\Phi(\omega)|^2$  was introduced[40, 49,

\*Electronic address: pvaro@otenet.gr

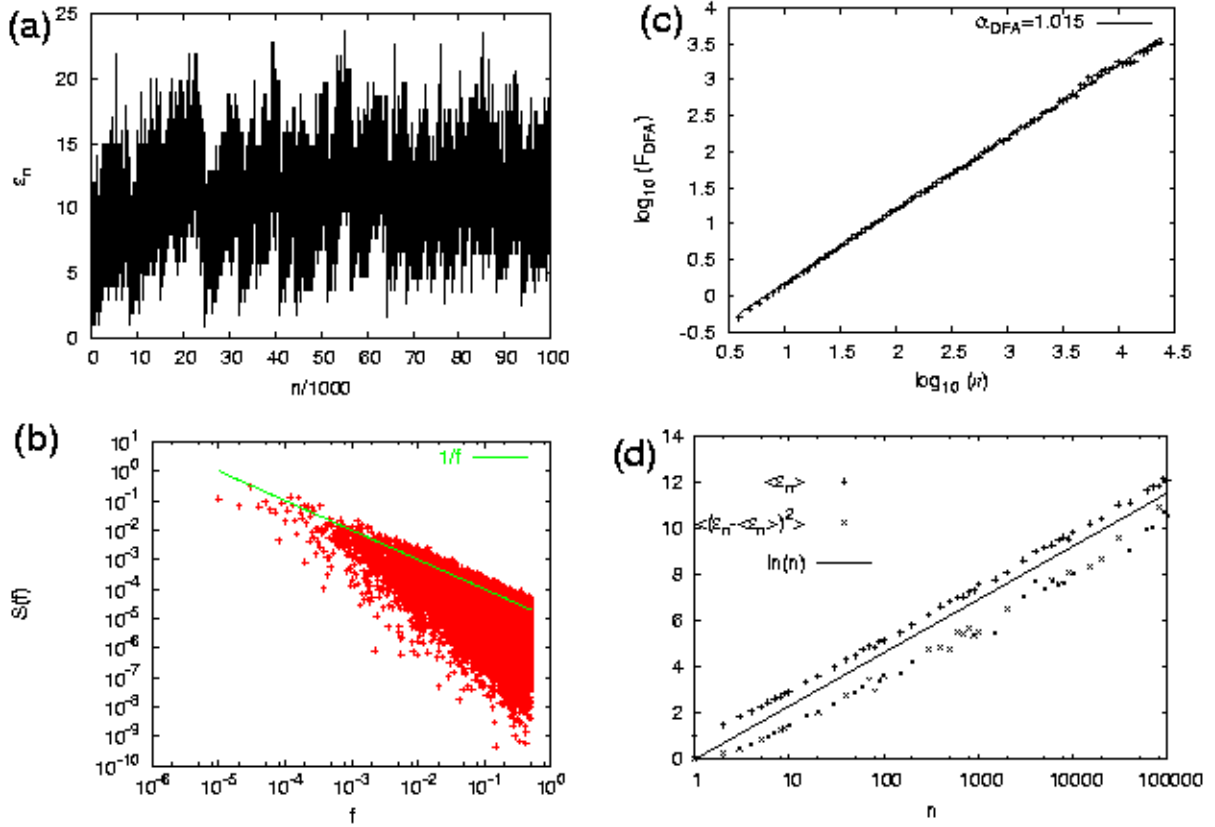


FIG. 1: (color online) (a): Example of the evolution of  $\epsilon_n$  (see the text) versus the number of renewals  $n$ , i.e., in natural time. (b): The Fourier power spectrum of (a); the (green) solid line corresponds to  $1/f$  and was drawn as a guide to the eye. (c): The DFA of (a) that exhibits an exponent  $\alpha_{DFA}$  very close to unity, as expected from (b). (d): Properties of the distribution of  $\epsilon_n$ . The average value  $\langle \epsilon_n \rangle$  (plus) and the variance  $\langle (\epsilon_n - \langle \epsilon_n \rangle)^2 \rangle$  (crosses) as a function of  $n$ . The straight solid line depicts  $\ln(n)$  and was drawn for the sake of reader's convenience.

50], where

$$\Phi(\omega) = \sum_{k=1}^N p_k \exp\left(i\omega \frac{k}{N}\right) \quad (1)$$

and  $p_k = Q_k / \sum_{n=1}^N Q_n$ ,  $\omega = 2\pi\phi$ ;  $\phi$  stands for the *natural frequency*. The continuous function  $\Phi(\omega)$  should *not* be confused with the usual discrete Fourier transform, which considers only its values at  $\phi = 0, 1, 2, \dots$ . In natural time analysis[36, 40, 49, 50], the properties of  $\Pi(\omega)$  or  $\Pi(\phi)$  are studied for natural frequencies  $\phi$  less than 0.5, since in this range of  $\phi$ ,  $\Pi(\omega)$  or  $\Pi(\phi)$  reduces to a *characteristic function* for the probability distribution  $p_k$  in the context of probability theory. When the system enters the *critical stage*, the following relation holds[40, 49, 56]:

$$\Pi(\omega) = \frac{18}{5\omega^2} - \frac{6 \cos \omega}{5\omega^2} - \frac{12 \sin \omega}{5\omega^3}. \quad (2)$$

For  $\omega \rightarrow 0$ , Eq.(2) leads to[36, 40, 49]

$$\Pi(\omega) \approx 1 - 0.07\omega^2$$

which reflects[56] that the variance of  $\chi$  is given by

$$\kappa_1 = \langle \chi^2 \rangle - \langle \chi \rangle^2 = 0.07,$$

where  $\langle f(\chi) \rangle = \sum_{k=1}^N p_k f(\chi_k)$ . The entropy  $S$  in the natural time-domain is defined as[49, 52]

$$S \equiv \langle \chi \ln \chi \rangle - \langle \chi \rangle \ln \langle \chi \rangle,$$

which depends on the sequential order of events[53, 54]. It exhibits[55] concavity, positivity, Lesche[62, 63] stability, and for *infinitely* ranged temporal correlations its value is smaller[36, 52] than the value  $S_u (= \ln 2/2 - 1/4 \approx 0.0966)$  of a “uniform” (u) distribution (as defined in Refs. [49, 51, 52, 53, 54], e.g. when all  $p_k$  are equal or  $Q_k$  are positive independent and identically distributed random variables of finite variance. In this case,  $\kappa_1$  and  $S$  are designated  $\kappa_u (= 1/12)$  and  $S_u$ , respectively.) Thus,  $S < S_u$ . The same holds for the value of the entropy obtained[55, 58] upon considering the time reversal  $\mathcal{T}$ , i.e.,  $\mathcal{T}p_k = p_{N-k+1}$ , which is labelled by  $S_-$ . In summary, the SES activities, when analyzed in natural time exhibit *infinitely* ranged temporal correlations and obey the conditions[58, 59]:

$$\kappa_1 = 0.07 \quad (3)$$

and

$$S, S_- < S_u. \quad (4)$$

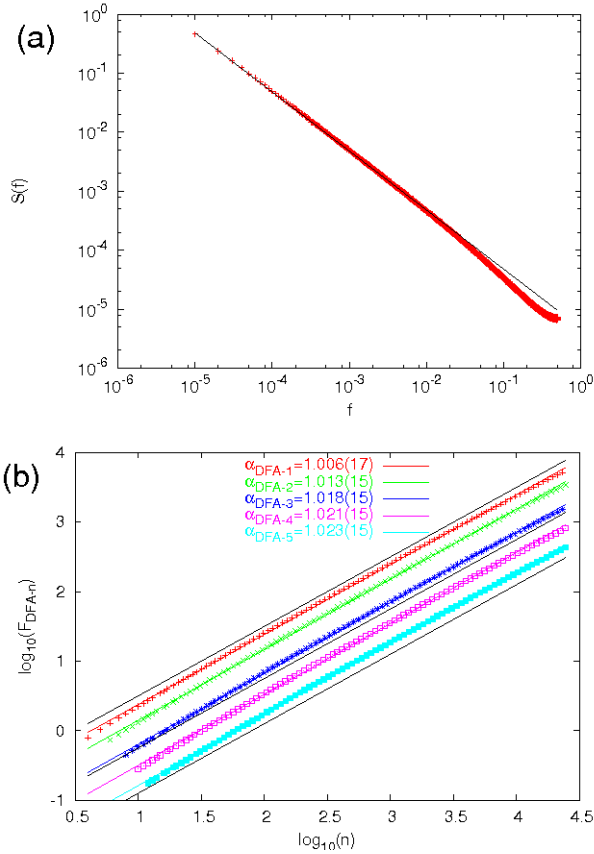


FIG. 2: (color online) Results from  $10^4$  runs of the model presented in Fig.1: (a) the average power spectrum, (b) Detrended Fluctuation Analyses of order  $n$  (DFA- $n$ ) [46]. The black solid line in (a) corresponds to  $1/f$  spectrum and was drawn as a guide to the eye. For the same reason in (b), the black solid lines correspond to  $\alpha_{DFA} = 1$ . In (b), the colored solid lines correspond to the least square fit of the average  $F_{DFA-n}$ , depicted by symbols of the same color; the numbers in parentheses denote the standard deviation of  $\alpha_{DFA-n}$  obtained from the  $10^4$  runs of the model. The various  $F_{DFA-n}$  have been displaced vertically for the sake of clarity.

The scope of the present paper is twofold. First, a simple model is proposed (Section II) which, in the frame of natural time, leads to  $1/f^a$  behavior with an exponent  $a$  close to unity. The properties of this model in natural time are compared to those of the SES activities in Section III. This comparison is carried out by making use of the most recent experimental data of SES activities observed in Greece during the last several months. Section IV presents the conclusions. Two Appendices are also provided the first of which refers to the earthquakes that followed the SES activities presented here. The second Appendix clarifies that an early model proposed by Voss [47] differs essentially than the one presented here.

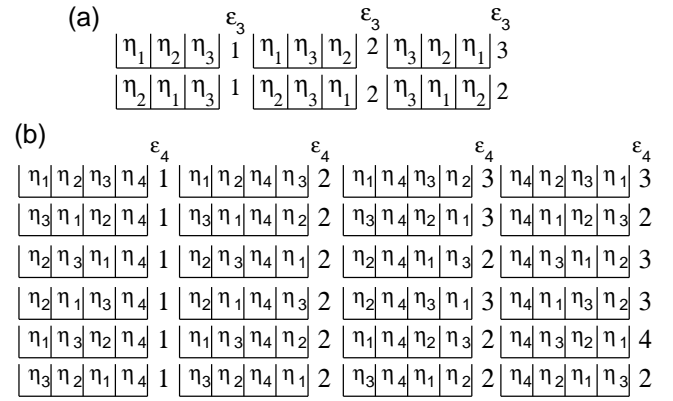


FIG. 3: The  $\eta_n$  values arranged in sites (bins) according to their value increasing from left to right. (a) The six ( $=3!$ ) equally probable outcomes after the selection of 3 random numbers by the same PDF. Actually, the sample space is (in one to one correspondence to) the permutations of 3 objects. (b) The 24 ( $=4!$ ) equally probable outcomes after the selection of 4 random numbers by the same PDF. Again, the sample space is (in one to one correspondence to) the permutations of 4 objects. For the reader's convenience, in each outcome, the corresponding  $\epsilon_n$ -value ( $n = 3$  or  $4$ ) is written. An inspection of (b), shows that  $p(\epsilon_4 = 1) = 1/4$ ,  $p(\epsilon_4 = 2) = 11/24$ ,  $p(\epsilon_4 = 3) = 1/4$  and  $p(\epsilon_4 = 4) = 1/24$ .

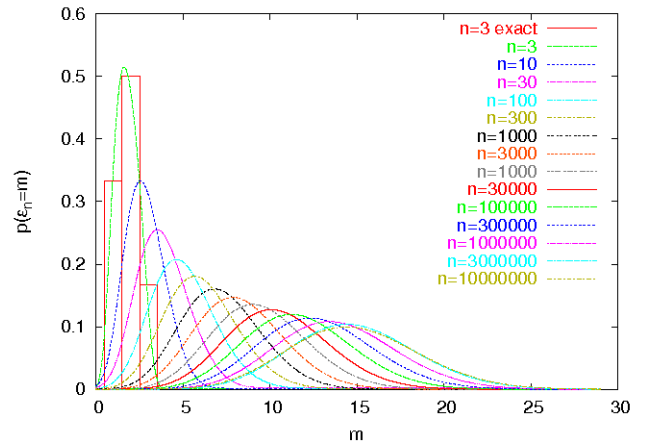


FIG. 4: (color online) The probabilities  $p(\epsilon_n = m)$  as a function of  $m$  for various  $n$ . The bar chart corresponds to the exact  $p(\epsilon_3 = m)$  whereas the continuous lines to the Cornish-Fisher approximation of Eq.(19). The latter approximation converges very rapidly to the true  $p(\epsilon_n = m)$ , see for example  $n = 3$ . This fact enables the calculation of  $p(\epsilon_n = m)$  for very large  $n$ , for which the recursive relation of Eq.(5) would accumulate significant round-off errors.

TABLE I: The values of  $S$ ,  $\kappa_1$ ,  $S_-$  for the electric signals presented in Fig.5.

Date recorded	$S$	$\kappa_1$	$S_-$
Feb 8, 2007	$0.067 \pm 0.007$	$0.074 \pm 0.007$	$0.079 \pm 0.007$
Apr 23, 2007	$0.071 \pm 0.005$	$0.069 \pm 0.003$	$0.066 \pm 0.005$
Apr 24, 2007	$0.072 \pm 0.003$	$0.067 \pm 0.003$	$0.069 \pm 0.003$
Nov 7, 2007	$0.070 \pm 0.005$	$0.065 \pm 0.005$	$0.070 \pm 0.005$

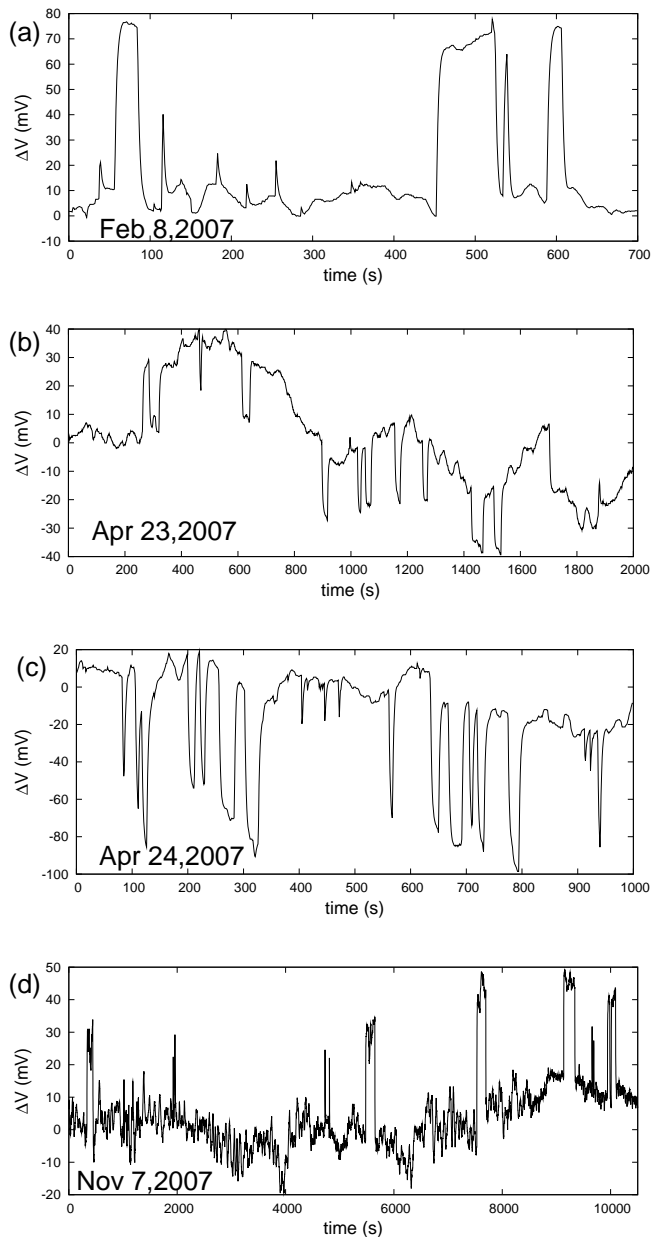


FIG. 5: Four electric signals recorded at PAT(sampling rate  $f_{exp}=1$  sample/sec) on February 8, 2007(a), April 23, 2007(b), April 24, 2007(c) and November 7, 2007(d).

## II. THE MODEL PROPOSED

### A. Description of the model

Here, we present a simple competitive evolution model which results, when analyzed in natural time, to  $1/f^a$  “noise” with  $a$  very close to unity. Let us consider the cardinality  $\epsilon_n$  of the family of sets  $S_n$  of successive extrema obtained from a given probability distribution function (PDF);  $S_0$  equals to the empty set. Each  $S_n$  is obtained by following the procedure described below for  $n$  times.

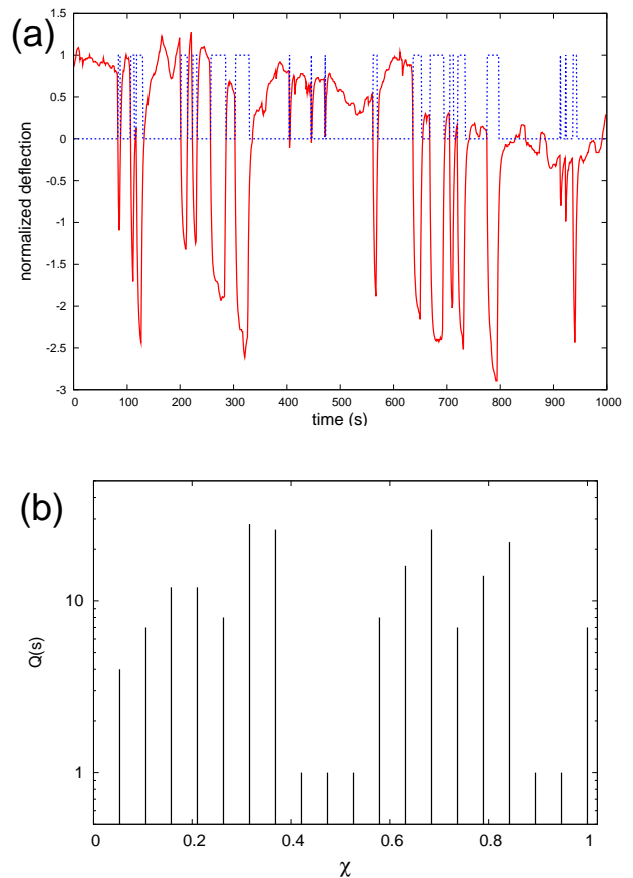


FIG. 6: (color online) (a): The electric signal depicted in Fig.5(c) (April 24,2007) in normalized units (i.e., by subtracting the mean value and dividing the results by the standard deviation) along with its dichotomous representation which is marked by the dotted (blue) line. (b): How the signal in (a) is read in natural time.

Select a random number  $\eta_n$  from a given PDF and compare it with all the numbers of  $S_{n-1}$ . In order to construct the set  $S_n$ , we disregard from the set  $S_{n-1}$  all its members that are smaller than  $\eta_n$  and furthermore include  $\eta_n$ . Thus,  $S_n$  is a finite set of real numbers whose members are always larger or equal to  $\eta_n$ . Moreover  $\min[S_n] \geq \min[S_{n-1}]$  and  $\max[S_n] \geq \max[S_{n-1}]$ . The cardinality  $\epsilon_n \equiv |S_n|$  of these sets, which may be considered as equivalent to the dimensionality of the thresholds distribution in the coherent noise model (e.g. see Ref.[64] and references therein), if considered as time-series with respect to the natural number  $n$  (see Fig.1(a), which was drawn by means of the *exponential* PDF) exhibits  $1/f^a$  noise with  $a$  very close to unity, see Fig.1(b). This very simple model whose evolution is depicted in Fig.1(a), leads to a Detrended Fluctuation Analysis[9] (DFA) exponent  $\alpha_{DFA}$  close to unity, see Fig.1(c), being compatible with the  $1/f$  power spectrum depicted in Fig.1(b). The mathematical model described above corresponds to an asymptotically non-stationary process, since  $\langle \epsilon_n \rangle \propto \ln n$  with a variance  $\langle (\epsilon_n - \langle \epsilon_n \rangle)^2 \rangle \propto \ln n$

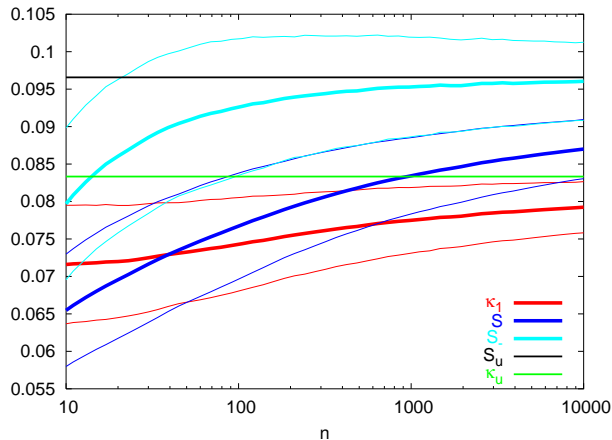


FIG. 7: (color online) Evolution of the parameters of  $\kappa_1$ ,  $S$  and  $S_-$  as a function of  $n$ , when  $\epsilon_n$  are analyzed in the natural time domain. The thick lines correspond to the average value of  $\kappa_1$ ,  $S$  and  $S_-$ , found by  $10^4$  runs of the model. The thinner lines correspond to the  $\pm$ one standard deviation confidence intervals. For the reader's convenience, the green and black horizontal lines show the values  $\kappa_u$  and  $S_u$  of  $\kappa_1$  and  $S$ , respectively, that correspond to a “uniform” distribution.

(see Fig.1(d)). Thus, in simple words, the present model suggests that the cardinality  $\epsilon_n$  of the family of sets  $S_n$  of successive extrema exhibits  $1/f^a$  behavior when considered as time-series with respect to the natural (time) number  $n$ . We note that a connection between  $1/f^a$  noise and extreme value statistics has been established and proposed as providing a new angle at the generic aspect of the phenomena[44]. Furthermore, in the frame of a formal similarity between the discrete spectrum of quantum systems and a discrete time series[14] the following striking similarity is noticed: The fact that  $a \approx 1$  together with the behavior  $\langle (\epsilon_n - \langle \epsilon_n \rangle)^2 \rangle \propto \ln n$  of the present model is reminiscent of the power law exponent and the  $\langle \delta_n^2 \rangle$  statistic in chaotic quantum systems[14, 15].

In order to check the stability of the results presented in Fig.1, we present in Fig.2(a) the average power spectrum obtained from  $10^4$  runs of the model. A sharp  $1/f$  behavior is observed. Moreover, in Fig.2(b), we present the results of the corresponding average values of  $F_{DFA-n}$  obtained from DFA of various orders  $n$  (i.e., when detrending with a polynomial of order  $n$ , see Ref.[46]). Figure 2(b) indicates that  $\alpha_{DFA-n}$  is close to unity.

## B. Analytical properties

We now discuss an analytical procedure which clarifies some properties of the model. In order to find analytically the distribution of the probabilities  $p(\epsilon_n)$ , one has simply to consider the possible outcomes when drawing  $n$  random numbers  $\eta_n$ . Since the selection is made by a means of a PDF, all these numbers are different from

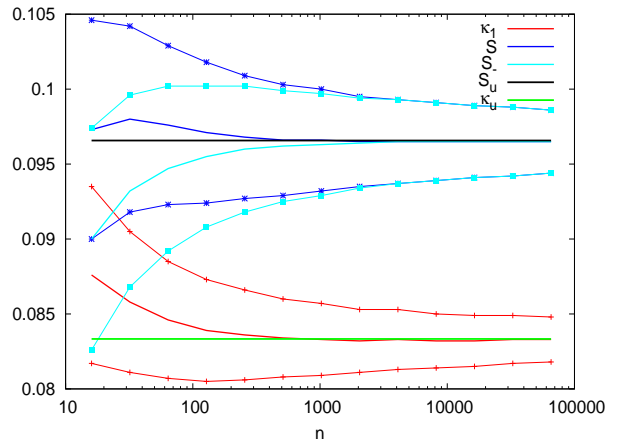


FIG. 8: (color online) Evolution of the parameters of  $\kappa_1$ ,  $S$  and  $S_-$  as a function of  $n$ , when  $v_n$  (see Appendix B) are analyzed in the natural time domain. Since the model produces  $1/f$  noise time series with lengths  $n = 2^m$ , the calculation was performed at such  $n$  (i.e.,  $n = 10^m$ ,  $m = 4, 5, \dots, 16$ ) indicated by the points marked. The thick lines connect the corresponding points of the average value of  $\kappa_1$ ,  $S$  and  $S_-$ , found by  $10^4$  runs of the model. The thinner lines connect the points corresponding to the  $\pm$ one standard deviation confidence intervals. For the reader's convenience, the green and black horizontal lines show the values  $\kappa_u$  and  $S_u$  of  $\kappa_1$  and  $S$ , respectively, that correspond to a “uniform” distribution. Here, as in Ref.[47], 6-sided dices ( $k = 6$ ) were considered.

each other, thus -when sorted they- are equivalent to  $n$  points (sites) lying on the real axis. The value of  $\epsilon_n$  varies as  $\{\eta_n\}$  permute along these  $n$  sites *independently* from the PDF used in the calculation. Thus, a detailed study of the permutation group of  $n$  objects can lead to an exact solution of the model. It is well known, however, that the number of the elements of this group is  $n!$  and this explains why we preferred to use the numerical calculation shown in Fig.1. Some exact results obtained by this method are the following:  $\langle \epsilon_1 \rangle = 1$ ;  $\langle \epsilon_2 \rangle = 1 + 1/2$ , since  $p(\epsilon_2 = 1) = p(\epsilon_2 = 2) = 1/2$ ;  $\langle \epsilon_3 \rangle = 1 + 1/2 + 1/3$ , since  $p(\epsilon_3 = 1) = 1/3$ ,  $p(\epsilon_3 = 2) = 1/2$  and  $p(\epsilon_3 = 3) = 1/6$ ;  $\langle \epsilon_4 \rangle = 1 + 1/2 + 1/3 + 1/4$  (see Fig.3). Figure 3 analyzes the results for  $n = 3$  (Fig.3(a)) and  $n = 4$  (Fig.3(b)). One can see that the probability  $p(\epsilon_n = m)$  equals to the sum of the  $n$  possible outcomes as  $\eta_n$  moves from the left to right in the  $n$  columns of Fig.3. In each column, the probability to have at the end  $\epsilon_n = m$  is just equal to the probability to keep  $m - 1$  numbers from the numbers already drawn that are larger than  $\eta_n$ . This results in

$$p(\epsilon_n = m) = \frac{1}{n} \sum_{k=m-1}^{n-1} p(\epsilon_k = m - 1) \quad (5)$$

(cf.  $p(\epsilon_0 = 0) = 1$ ).

Equation (5) enables us to calculate the characteristic

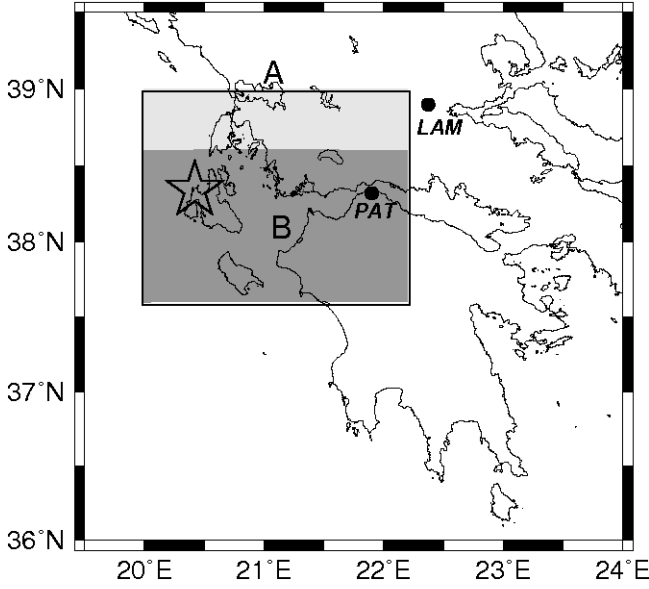


FIG. 9: The map shows the areas A,B. The star indicates the epicenter of the strong 6.0 EQ that occurred on March 25, 2007 in Kefallonia.

function (see p.928 of Ref.[65])

$$f_n(\lambda) \equiv \langle \exp(\lambda \epsilon_n) \rangle = \sum_{m=1}^n e^{\lambda m} p(\epsilon_n = m). \quad (6)$$

Indeed, by substituting  $p(\epsilon_n = m)$  in  $f_n(\lambda)$ , we obtain

$$n f_n(\lambda) = \sum_{m=1}^n e^{\lambda m} \sum_{k=m-1}^{n-1} p(\epsilon_k = m-1), \quad (7)$$

whereas by substituting  $p(\epsilon_{n+1} = m)$  in  $f_{n+1}(\lambda)$ , we find

$$(n+1)f_{n+1}(\lambda) = \sum_{m=1}^n e^{\lambda m} \sum_{k=m-1}^{n-1} p(\epsilon_k = m-1) + e^{\lambda} f_n(\lambda). \quad (8)$$

Subtracting now Eq.(7) from Eq.(8), we finally get

$$f_{n+1}(\lambda) = \frac{n + e^{\lambda}}{n + 1} f_n(\lambda). \quad (9)$$

Since  $f_1(\lambda) = e^{\lambda}$ , we find that Eq.(9) -upon considering Eq.6.1.22 of Ref.[65]- results in

$$f_n(\lambda) = \frac{1}{n!} \frac{\Gamma(e^{\lambda} + n)}{\Gamma(e^{\lambda})}, \quad (10)$$

where  $\Gamma(x)$  is the gamma function. Now, the mean and all the central moments  $\mu_l \equiv \langle (\epsilon_n - \langle \epsilon_n \rangle)^l \rangle$  of the distribution of  $p(\epsilon_n = m)$  can be obtained by virtue of the

cumulant theorem (see p.928 of Ref.[65]):

$$\langle \epsilon_n \rangle = \left. \frac{d}{d\lambda} \ln f_n(\lambda) \right|_{\lambda=0}, \quad (11)$$

$$\mu_2 \equiv \langle (\epsilon_n - \langle \epsilon_n \rangle)^2 \rangle = \left. \frac{d^2}{d\lambda^2} \ln f_n(\lambda) \right|_{\lambda=0}, \quad (12)$$

$$\mu_3 \equiv \langle (\epsilon_n - \langle \epsilon_n \rangle)^3 \rangle = \left. \frac{d^3}{d\lambda^3} \ln f_n(\lambda) \right|_{\lambda=0}, \quad (13)$$

$$\mu_4 - 3\mu_2^2 = \left. \frac{d^4}{d\lambda^4} \ln f_n(\lambda) \right|_{\lambda=0}. \quad (14)$$

Substituting Eq.(10) into Eqs.(11) to (14) and using the properties of the polygamma functions (i.e., the n-th order logarithmic derivatives of the gamma function, see p.260 of Ref.[65]), we obtain

$$\langle \epsilon_n \rangle = \sum_{k=1}^n \frac{1}{k}, \quad (15)$$

$$\langle (\epsilon_n - \langle \epsilon_n \rangle)^2 \rangle = \sum_{k=1}^n \left( \frac{1}{k} - \frac{1}{k^2} \right), \quad (16)$$

$$\mu_3 = \sum_{k=1}^n \left( \frac{1}{k} - \frac{3}{k^2} + \frac{2}{k^3} \right), \quad (17)$$

$$\mu_4 - 3\mu_2^2 = \sum_{k=1}^n \left( \frac{1}{k} - \frac{7}{k^2} + \frac{12}{k^3} - \frac{6}{k^4} \right). \quad (18)$$

Equations (15) to (18) enable us to calculate the mean, standard deviation  $\sigma (= \sqrt{\mu_2})$ , skewness  $\gamma_1 = \mu_3/\sigma^3$  and kurtosis  $\gamma_2 = \mu_4/\sigma^4 - 3$  as a function of  $n$ . Using now the Cornish-Fisher (CF) expansion treated in Ref.[66], we obtain the following continuous approximation to  $p(\epsilon_n = m)$

$$p_{CF}(\tilde{\epsilon}_n) = \frac{1}{\sqrt{2\pi}} \left| 1 - \frac{\gamma_1}{3} \tilde{\epsilon}_n + \frac{\gamma_1^2}{36} (12\tilde{\epsilon}_n^2 - 7) - \frac{\gamma_2}{8} (\tilde{\epsilon}_n^2 - 1) \right| \times \exp \left\{ -\frac{1}{2} \left[ \tilde{\epsilon}_n - \frac{\gamma_1}{6} (\tilde{\epsilon}_n^2 - 1) - \frac{\gamma_2}{24} (\tilde{\epsilon}_n^3 - 3\tilde{\epsilon}_n) + \frac{\gamma_1^2}{36} (4\tilde{\epsilon}_n^3 - 7\tilde{\epsilon}_n) \right]^2 \right\}$$

where  $\tilde{\epsilon}_n = (\epsilon_n - \langle \epsilon_n \rangle)/\sigma$ . Equation (19), although being a continuous approximation to the point probabilities  $p(\epsilon_n = m)$ , rapidly converges to the latter, see for example the comparison of the exact  $p(\epsilon_3 = m)$  and the corresponding  $p_{CF}(\tilde{\epsilon}_3)/\sigma$  in Fig.4. An inspection of this figure, which depicts the probabilities  $p(\epsilon_n = m)$  up to  $n = 10^7$ , reveals that even for large  $n$ , the probability  $p(\epsilon_n = m)$  remains non-Gaussian (cf. even at  $n = 10^9$ , we obtain from Eqs.(16) to (18)  $\gamma_1 = 0.2154 \neq 0$  with  $\gamma_2 = 0.0459 \neq 0$ ).

### III. COMPARISON OF THE MODEL WITH THE SES PHYSICAL PROPERTIES IN NATURAL TIME

We first present in III A the most recent experimental results on Seismic Electric Signals and then compare in

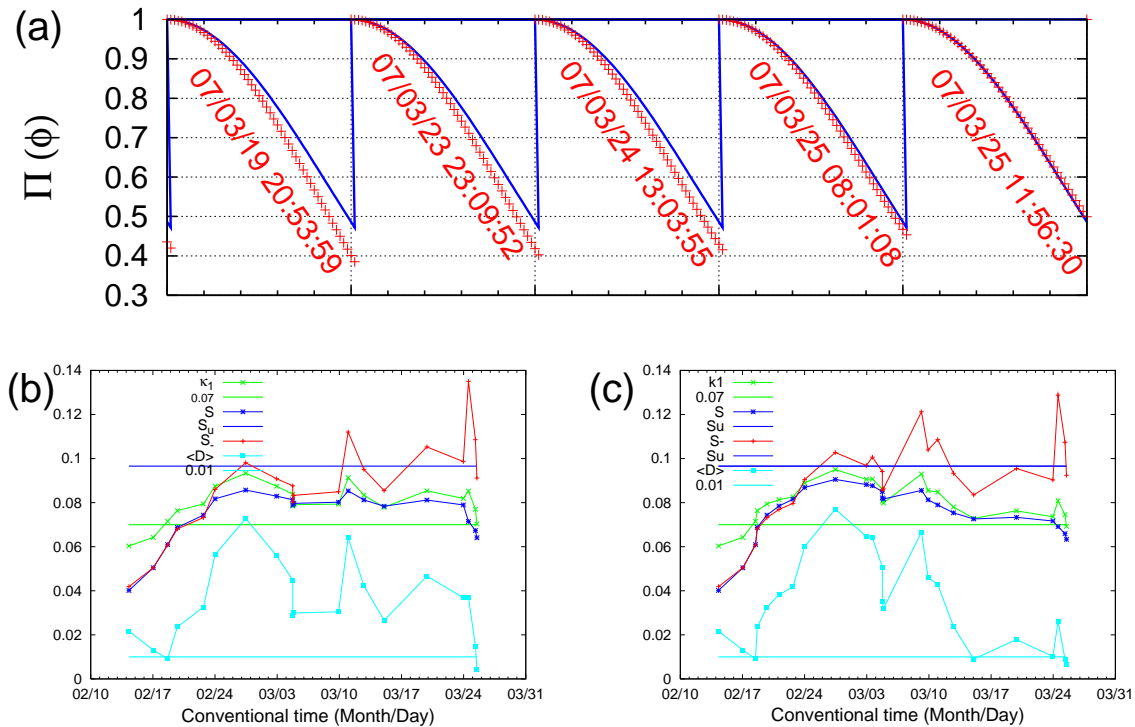


FIG. 10: (color online) (a) The normalized power spectrum (red)  $\Pi(\phi)$  of the seismicity as it evolves event by event (whose date and time (UT) of occurrence are written in each panel) after the initiation of the SES activity on February 8, 2007. The excerpt presented here refers to the period 19 to 25 March, 2007 and corresponds to the area B,  $M_{thres} = 3.2$ . In each case only the spectrum in the area  $\phi \in [0, 0.5]$  is depicted (separated by the vertical dotted lines), whereas the  $\Pi(\phi)$  of Eq.(2) is depicted by blue color. The minor horizontal ticks for  $\phi$  are marked every 0.1. (b), (c) Evolution of the parameters  $\langle D \rangle$ ,  $\kappa_1$ ,  $S$  and  $S_-$  after the initiation of the SES activity on February 8, 2007 for the areas B ( $M_{thres} = 3.2$ ) and A ( $M_{thres} = 3.2$ ), respectively, until just before the 6.0 EQ.

IIIB their properties with the results of the model proposed.

#### A. The recent electric field data

Figure 5 depicts the original time series of four electrical disturbances that have been recently recorded on: (a) February 8, 2007, (b) April 23, 2007, (c) April 24, 2007 and (d) November 7, 2007 at a measuring station termed Patras (PAT) located at  $\approx 160$ km west of Athens. All these four recent signals were analyzed in natural time. For example, if we read in natural time the signal on April 24, 2007 (Fig.5(c)) -the dichotomous representation of which is marked by the dotted (blue) line in Fig.6(a)-we find the natural time representation of Fig.6(b) the analysis of which leads to the values  $\kappa_1 = 0.067 \pm 0.003$ ,  $S = 0.072 \pm 0.003$ ,  $S_- = 0.069 \pm 0.003$ . The relevant results of all the four signals are compiled in Table I and found to be consistent with the conditions (3) and (4), thus they can be classified as SES activities (for their subsequent seismicity as well as for more recent SES activities see Appendix A). An inspection of Table I shows that the  $S$  value is more or less comparable to that of  $S_-$ , but experimental uncertainty does not allow any conclu-

sion which of them is larger. Note that in several former examples[55], the data analysis also showed that the  $S$  value may either be smaller or larger than  $S_-$ .

#### B. Comparison of the SES properties with those of the model proposed

We now turn to investigate whether the parameters  $\kappa_1$ ,  $S$  and  $S_-$  deduced from the  $1/f$  model of Section II are consistent to those resulted from the analysis of the SES activities observed. Figure 7 summarizes the results of  $10^4$  runs of the model which, for moderate sizes of  $n$ , seems to obey more or less the conditions (3) and (4). In particular, for  $n \lesssim 10^2$  (which is frequently the number of pulses of the SES activities observed in field experiments), Fig.7 shows that  $\kappa_1$  is close to 0.070,  $S < S_u$  and (in most cases)  $S_- < S_u$ . A closer inspection of Fig.7, however, reveals the following incompatibility of the model with the experimental results: For  $n \lesssim 10^2$ , the model clearly suggests that  $S_- > S$ , thus disagreeing with the experimental data which show, as mentioned above, that  $S$  may either be smaller or larger than  $S_-$ . The origin of this incompatibility has not been fully understood. It might be due to the fact that SES activities

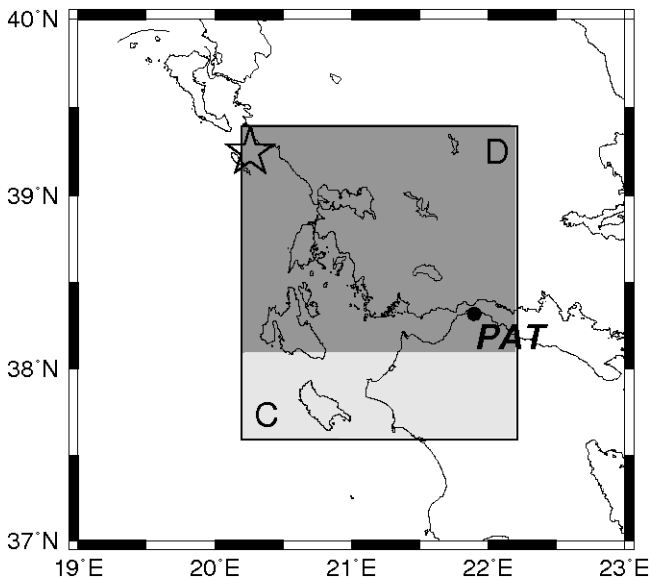


FIG. 11: The map shows the areas C and D. The star shows the epicenter of the strong 5.8 EQ at 18:09:11 on June 29, 2007.

exhibit *critical* dynamics, while the model cannot capture all the characteristics of such dynamics.

Since the model proposed here might be considered as reminiscent of an early model proposed by Voss (see Ref.[47]), which is also a discrete one, we also present in Fig.8 the corresponding results of  $10^4$  runs of that model. (The details are given in the Appendix B). A comparison of Figs.7 and 8 for  $n \leq 10^2$  reveals that the results of the two models differ essentially. For example, in the Voss model,  $S_-$  is larger than  $S_u$  while the opposite holds for the model proposed here. Moreover, when comparing the results of the Voss model with those of the SES activities we also find considerable differences. For example, the  $\kappa_1$  value deduced from the Voss model is (on the average) *larger* than  $\kappa_u$ , thus differing considerably from the value  $\kappa_1 \approx 0.070$  of the SES activities. This, as mentioned above, is comparable to the one deduced from the model proposed here and explains why we focused on this paper on the comparison of that model -among the variety of models suggested to date for the explanation of the  $1/f$  behavior- with the experimental values obtained from the analysis of the SES activities

#### IV. CONCLUSIONS

In summary, using the newly introduced concept of natural time:(a) A simple model is proposed that exhibits  $1/f^a$  behavior with  $a$  close to unity. (b) Electric signals, recorded during the last few months in Greece, are classified as SES activities since they exhibit *infinitely* ranged temporal correlations. Actually, three magnitude 6.0 class earthquakes already occurred in Greece (see the Appendix). (c) For sizes  $n$  comparable to those of the

SES activities measured in the field experiments (i.e.,  $n \lesssim 10^2$ ), the model proposed here leads to values of the parameters  $\kappa_1$  ( $\approx 0.070$ ) and  $S, S_- (< S_u)$  that are consistent with those deduced from the SES activities analysis. Despite of this fact, however, the model results in  $S_-$  values that are almost always larger than those of  $S$ , while the observed SES activities result in  $S$  values that may either be larger or smaller than  $S_-$ . This discrepancy might be due to the inability of the model to capture the characteristics of *critical* dynamics which is exhibited by SES activities.

#### APPENDIX A: WHAT HAPPENED AFTER THE SES ACTIVITIES DEPICTED IN FIG.5

We clarify that, during the last decade, preseismic information[67] based on SES activities is issued *only* when the magnitude of the strongest EQ of the impending EQ activity is estimated -by means of the SES amplitude[26, 27, 28, 29, 30] to be comparable to 6.0 units or larger[36].Here,in the first two subsections, we explain what happened after the SES activity at PAT on February 8, 2007 (see Fig.5(a)) and on April 23 and 24, 2007 (see Figs.5(b),(c)). The relevant analysis of seismicity after the SES activity on November 7, 2007, which was still in progress[48] during the submission of this paper on 23 November, 2007 and hence completed afterwards, is presented in Subsection 3.

##### 1. What happened after the SES activity of February 8, 2007

According to the Athens observatory (the seismic data of which will be used here), a strong earthquake (EQ) with magnitude 6.0-units occurred at Kefallonia area, i.e.,  $38.34^\circ\text{N } 20.42^\circ\text{E}$ , at 13:57 UT on March 25, 2007. We show below that the occurrence time of this strong EQ can be estimated by following the procedure described in Refs.[36, 49, 56, 58, 59].

We study how the seismicity evolved after the recording of the SES activity at PAT on February 8, 2007, by considering either the area A: $N_{37.6}^{39.0} E_{20.0}^{22.2}$  or its smaller area B: $N_{37.6}^{38.6} E_{20.0}^{22.2}$  (see Fig.9). If we set the natural time for seismicity zero at the initiation of the SES activity on February 8, 2007, we form time series of seismic events in natural time for various time windows as the number  $N$  of consecutive (small) EQs increases. We then compute the normalized power spectrum in natural time  $\Pi(\phi)$  for each of the time windows. Excerpt of these results, which refers to the values deduced during the period from 20:53:59 UT on March 19, 2007, to 11:56:30 UT on 25 March, 2007, is depicted in red in Fig.10(a). This figure corresponds to the area B with magnitude threshold (hereafter referring to the local magnitude ML or the ‘duration’ magnitude MD)  $M_{thres} = 3.2$ . In the same figure, we plot in blue the power spectrum obeying the

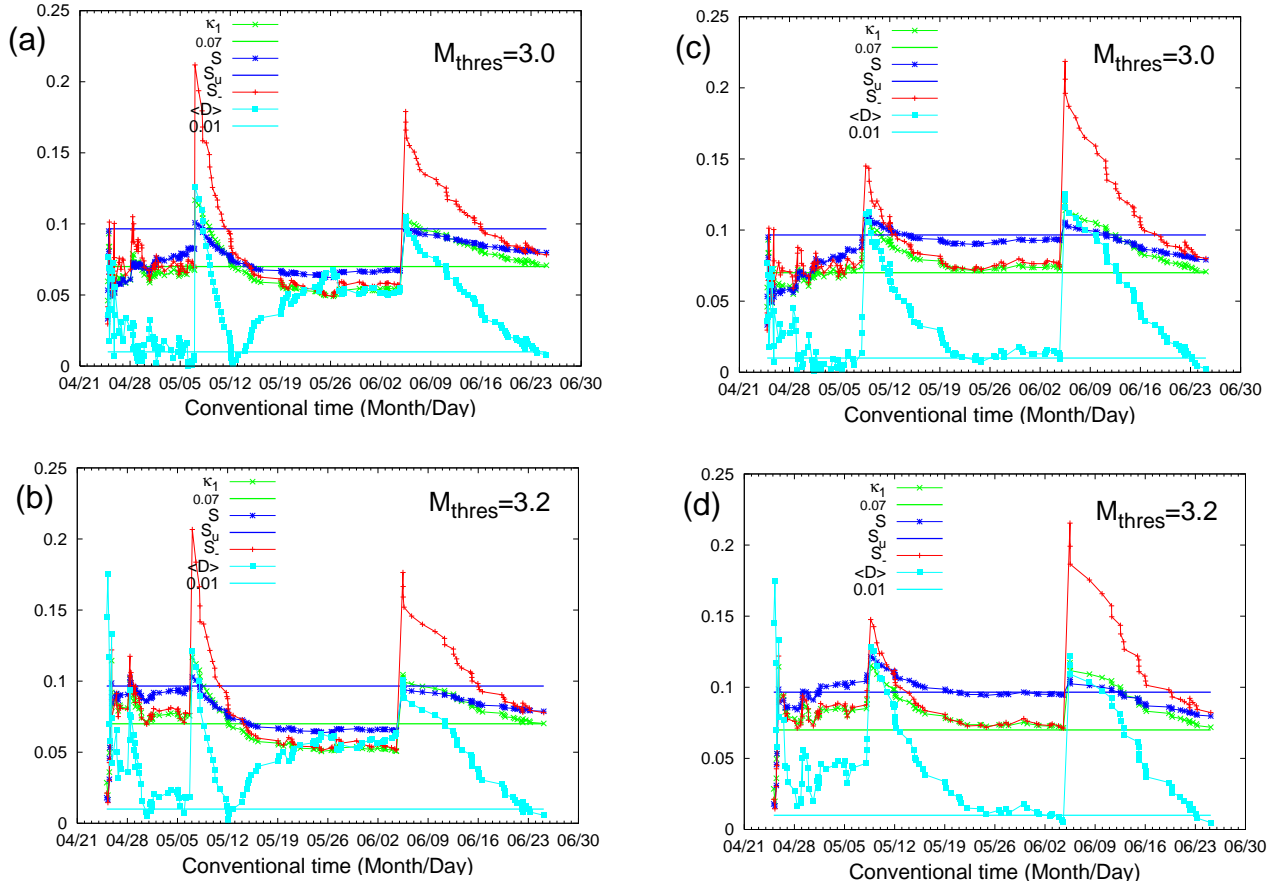


FIG. 12: (color online) (a),(b) and (c),(d) depict the evolution of the parameters  $\langle D \rangle$ ,  $\kappa_1$ ,  $S$  and  $S_-$  after the initiation of the SES activity on April 24, 2007 for the areas C and D, respectively (for two magnitude thresholds in each area), until 03:40:15 UT on June 25, 2007.

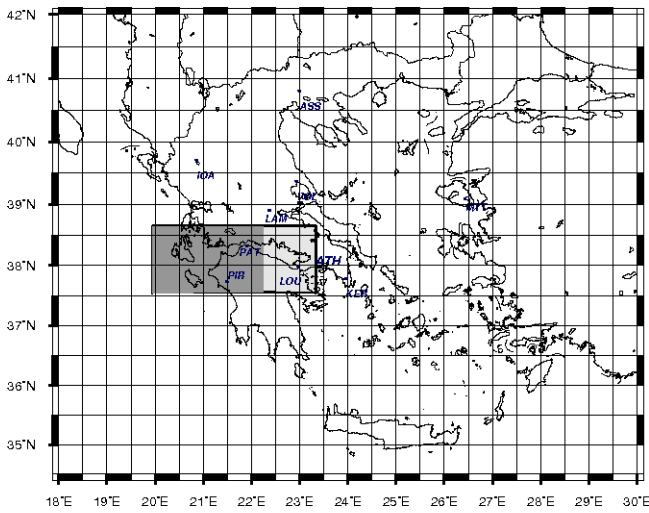


FIG. 13: (color online) The map shows the areas  $N_{38.6}^{37.6} E_{22.2}^{20.0}$  and  $N_{37.6}^{38.6} E_{20.0}^{23.3}$  in which the seismicity was studied[48] after the SES activity recorded at PAT on 7 November, 2007. The solid dots stand for the sites at which electric field variations are continuously monitored with a sampling frequency  $1\text{Hz}$

relation (2) which holds, as mentioned, when the system enters the *critical* stage. The date and the time of the occurrence of each small earthquake (with magnitude exceeding (or equal to) the aforementioned threshold) that occurred in area B, is also written in red in each panel. An inspection of this figure reveals that the red line approaches the blue line as  $N$  increases and a *coincidence* occurs at the last small event which had a magnitude 3.2 and occurred at 11:56:30 UT on March 25, 2007, i.e., just two hours before the strong 6.0 EQ. To ensure that this coincidence is a *true* one (see also below) we also calculate the evolution of the quantities  $\kappa_1, S$  and  $S_-$  and the results are depicted in Fig. 10(b) and 10(c) for the same magnitude thresholds for each of the areas B and A, respectively.

The conditions for a coincidence to be considered as *true* are the following (e.g., see Refs.[36, 49, 56, 58, 59]): First, the ‘average’ distance  $\langle D \rangle$  between the empirical and the theoretical  $\Pi(\phi)$  (i.e., the red and the blue line, respectively, in Fig.10(a)) should be smaller than  $10^{-2}$ . See Fig. 10(b),(c) where we plot  $\langle D \rangle$  versus the conventional time for the aforementioned two areas B and A, respectively. Second, in the examples observed to date,

a few events *before* the coincidence leading to the strong EQ, the evolving  $\Pi(\phi)$  has been found to approach that of the relation (2), i.e., the blue one in Fig.10(a), from *below* (cf. this reflects that during this approach the  $\kappa_1$ -value decreases as the number of events increases). In addition, both values  $S$  and  $S_-$  should be smaller than  $S_u$  at the coincidence. Finally, since the process concerned is self-similar (*critical* dynamics), the time of the occurrence of the (true) coincidence should *not* change, in principle, upon changing the surrounding area (and the magnitude threshold  $M_{thres}$ ) used in the calculation. Note that in Fig. 10(b), upon the occurrence of the aforementioned last small event at 11:56:30 UT of March 25, 2007, in area B the  $\langle D \rangle$  value becomes smaller than  $10^{-2}$ . The same was found to hold for the area A, see Fig.10(c).

## 2. What happened after the SES activities of April 23 and 24, 2007

We investigate the seismicity after the aforementioned SES activities depicted in Figs.5(b) and 5(c). The investigation is made in the areas C:  $N_{37.6}^{39.4}E_{20.2}^{22.2}$  and D:  $N_{38.1}^{39.4}E_{20.2}^{22.2}$  (see Fig.11). Starting the computation of seismicity from the initiation of the SES activity on April 24, 2007 (which, between the two SES activities depicted in Figs.5(b) and 5(c), has the higher actual amplitude), we obtain the results depicted in Figs.12(a),(b) and 12(c),(d) for the areas C and D, respectively, for  $M_{thres} = 3.0$  and  $M_{thres} = 3.2$ . An inspection of the parameters  $\langle D \rangle$ ,  $\kappa_1$ ,  $S$  and  $S_-$  reveals that they exhibited a *true* coincidence (as discussed above) around June 25, 2007, i.e., around four days before the 5.8 EQ that occurred at 18:09:11 UT on June 29, 2007, with an epicenter at 39.3°N 20.3°E (shown by a star in Fig.11).

## 3. Study of the seismicity after the SES activity on November 7, 2007

This study, which as mentioned above was still in progress upon the submission of the previous version of this paper, was made by investigating the seismicity in the area B of Fig.9, i.e.,  $N_{37.6}^{38.6}E_{20.0}^{22.2}$  as well as in the larger area, i.e.,  $N_{37.6}^{38.6}E_{20.0}^{23.3}$  (see Ref.[48]), which are shown in Fig.13. The parameters  $\kappa_1$ ,  $S$ ,  $S_-$  and  $\langle D \rangle$  computed during the subsequent period for  $M_{thres} = 3.1$  are depicted in Figs 14(a) and 14(b) for the smaller and larger area, respectively. An inspection of these two figures reveals that the conditions for a *true* coincidence (see subsection A.2) were obeyed upon the occurrence of the first event early in the morning (i.e., at 03:25 UT) on 30 December, 2007 with an epicenter at 37.8°N 20.2°E and magnitude 3.9. Almost three hours later, i.e., at 06:42 UT, a strong earthquake of magnitude 5.3 occurred at 37.6°N 20.9°E marked with the small star in Fig.15. In addition, and quite interestingly, the four parameters  $\kappa_1$ ,  $S$ ,  $S_-$  and  $\langle D \rangle$  during the next few days continued to ful-

fill the conditions for a true coincidence, as it is evident from a closer inspection of Figs.14(a) and 14(b). Actually, at 05:14 UT on 6 January, 2008, a major magnitude 6.6 earthquake occurred, which was felt not only all over Greece but also in adjacent countries, e.g., southern Italy and western Turkey. Its epicenter, marked with a large star in Fig.15, was located at 37.1°N 22.8°E, i.e., only around 50 km to the south of the larger area studied since the submission of the previous version of this paper[48]. Interestingly, in the part of the latter area adjacent to the epicenter (which is shaded in Fig.15) the four parameters  $\kappa_1$ ,  $S$ ,  $S_-$  and  $\langle D \rangle$  reached the conditions for a true coincidence just in the morning (i.e., at 04:24 UT) of 5 January, 2008 upon the occurrence of a magnitude 3.5 earthquake at 38.4°N 22.0°E (it corresponds to the last point in Fig.14(c) where  $\langle D \rangle$  becomes smaller than 1%).

Finally, we note that *after* the submission of the present paper, two additional SES activities have been recorded as follows (see Fig.16): One SES activity at PAT on 10 January, 2008 and another one on 14 January, 2008 at the station PIR located in western Greece, see Fig.13 (cf. The configuration of the measuring dipoles in the latter station is described in detail in the EPAPS document of Ref.[59]). Their subsequent seismicities are currently studied along the lines explained above considering the evolving seismicity in the following areas: Concerning the former SES activity at PAT the areas depicted in Fig.13, while for the one at PIR on 14 January, 2008, the subsequent seismicity is studied in the area B of Fig.9 as well as in the larger area  $N_{36.0}^{38.6}E_{20.0}^{22.0}$ .

We now offer some comments on the classification of the aforementioned electric signals of Fig 15 as SES activities. Concerning the signal on 14 January, 2008, which is of clear dichotomous nature, the analysis is made by considering that  $Q_k$  stands for the duration of  $k$ -th pulse, as mentioned in Section I, and the following parameters are obtained:  $\kappa_1 = 0.070$ ,  $S = 0.086$ ,  $S_- = 0.070$ , which obey the conditions (3) and (4) for the classification of the signal as SES activity. Furthermore, note the  $S_-$  is smaller than that of  $S$ , which is not compatible with the model proposed in Section II, thus strengthening the point mentioned in Section III.B as well as in the Conclusions (Section IV) that the model does not seem to capture the characteristics of critical dynamics exhibited by SES activities. We now turn to the signal recorded at PAT on 10 January, 2008, the feature of which is not clearly dichotomous since it consists of three main pulses that seem to overlap. Its analysis leads to the following values  $\kappa_1 = 0.070$ ,  $S = 0.050$ ,  $S_- = 0.060$ . These values, which are *different* from those deduced from the analysis of the SES activity on 7 November, 2007, also obey the conditions (3) and (4). At this point we clarify that the optimality of natural time domain for enhancing the signal's localization in the time-frequency space was shown[61] without assuming that  $Q_k$  stands for the pulse duration, but it was noted that in general  $Q_k$  is a quantity proportional to the corresponding energy released in the  $k$ -th event (cf. If pulses of very short duration ex-

ist, the calculation of  $Q_k$  should necessarily consider the characteristics of the low pass filters used in our measurements that have been described in detail in the EPAPS document of Ref.[60]).

### APPENDIX B: COMPARISON OF THE PRESENT MODEL WITH A MODEL SUGGESTED BY R.F.VOSS

A model producing  $1/f$  noise, suggested by Richard F. Voss, was presented in Ref.[47]. This model assumes some number  $m$  of  $k$ -sided dices, i.e., the outcome of a rolling the  $l$ -th dice is equally distributed among the values  $d_l = 1, 2, \dots, k$ . To each dice  $l$ , one relates the  $l$ -th digit of the binary representation of a number  $n = 0, 1, \dots, 2^m - 1$ . The procedure to generate the  $1/f$  noise starts ( $n = 0$ ) by rolling all dice and assign their sum to  $v_0 (= \sum_{l=1}^m d_l)$ . In the second step ( $n = 1$ ), one rerolls only the dice associated with the first digit of the binary representation, and the new roll  $d'_1$  is summed with the previous rolls of all other dices so that  $v_1 = d'_1 + \sum_{l=2}^m d_l$ . The procedure continues up to  $n = 2^m - 1$ , each time rolling only the dices associated with the digits that change when considering the binary representation of  $n$  compared to  $n - 1$ . This model results in time-series  $v_n$  of length  $2^m$  whose spectrum is close to  $1/f$ , and their values  $v_n$  are obviously distributed among the integers  $m$  and  $mk$ . The time series  $v_n$  clearly differ

from  $\epsilon_n$  apart from the fact that they both have integer values. To visualize this difference, we depict in Fig.17 the distribution of  $p(v_{2^m-1})$  for the case of 6-sided dices ( $k = 6$ ). It can be easily found, since upon considering the binary representation of  $n = 2^m - 1$  compared to  $n - 1 = 2^m - 1 - 1$ , all the digits change and one rerolls all dices. Clearly, rolling all dices results in a symmetric (*skewnessless*) distribution for  $v_{2^m-1}$  (see Fig.17). Indeed, by considering the distribution of the sum of rolling  $m$  independent  $k$ -sided dices and using the characteristic function method discussed in subsection IIB, one can find the following cumulants:

$$\langle v_{2^m-1} \rangle = m \frac{k+1}{2} \quad (\text{B1})$$

$$\langle (v_{2^m-1} - \langle v_{2^m-1} \rangle)^2 \rangle = m \frac{(k^2 - 1)}{12} \quad (\text{B2})$$

$$\langle (v_{2^m-1} - \langle v_{2^m-1} \rangle)^3 \rangle = 0 \quad (\text{B3})$$

$$\langle (v_{2^m-1} - \langle v_{2^m-1} \rangle)^4 \rangle - 3 \langle (v_{2^m-1} - \langle v_{2^m-1} \rangle)^2 \rangle^2 = m \frac{(1 - k^4)}{120} \quad (\text{B4})$$

Clearly, Eqs.(B1) to (B4) for the distribution of  $v_{2^m-1}$  differ from Eqs.(15) to (18) for the distribution of  $\epsilon_n$ . Among their differences, the following two are the most striking: First,  $v_{2^m-1}$  is skewnessless whereas that of  $\epsilon_n$  is not, and second the two distributions have different signs in their kurtoses.

- 
- [1] B. B. Mandelbrot, *Multifractals and 1/f Noise* (Springer-Verlag, New York, 1999).
- [2] T. Antal, M. Droz, G. Györgyi, and Z. Rácz, Phys. Rev. E **65**, 046140 (2002).
- [3] M. B. Weissman, Rev. Mod. Phys. **60**, 537 (1988).
- [4] T. Musha and H. Higuchi, Jpn. J. Appl. Phys. **15**, 1271 (1976).
- [5] K. Nagel and M. Paczuski, Phys. Rev. E **51**, 2909 (1995).
- [6] X. Zhang and G. Hu, Phys. Rev. E **52**, 4664 (1995).
- [7] A. Nakahara and T. Isoda, Phys. Rev. E **55**, 4264 (1997).
- [8] A. L. Goldberger, L. A. N. Amaral, J. M. Hausdorff, P. C. Ivanov, C.-K. Peng, and H. E. Stanley, Proc. Natl. Acad. Sci. USA **99**, 2466 (2002).
- [9] C.-K. Peng, J. Mietus, J. M. Hausdorff, S. Havlin, H. E. Stanley, and A. L. Goldberger, Phys. Rev. Lett. **70**, 1343 (1993).
- [10] S. Mercik, K. Weron, and Z. Ziwy, Phys. Rev. E **60**, 7343 (1999).
- [11] B. Mandelbrot and J. R. Wallis, Water Resour. Res. **5**, 321 (1969).
- [12] F. Lillo and R. N. Mantegna, Phys. Rev. E **62**, 6126 (2000).
- [13] J. M. G. Cómez, A. Relaño, J. Retamosa, E. Faleiro, L. Salasnich, M. Vraničar, and M. Robnik, Phys. Rev. Lett **94**, 084101 (2005).
- [14] A. Relaño, J. M. G. Cómez, R. A. Molina, J. Retamosa, and E. Faleiro, Phys. Rev. Lett **89**, 244102 (2002).
- [15] M. S. Santhanam and J. N. Bandyopadhyay, Phys. Rev. Lett. **95**, 114101 (2005).
- [16] M. S. Santhanam, J. N. Bandyopadhyay, and D. Angom, Phys. Rev. E **73**, 015201 (2006).
- [17] W. H. Press, Comments Astrophys. **7**, 103 (1978).
- [18] D. L. Gilder, T. Thornton, and M. W. Mallon, Science **267**, 1837 (1995).
- [19] H. Yoshinaga, S. Miyazima, and S. Mitake, Physica A **280**, 582 (2000).
- [20] J. M. Berger and B. B. Mandelbrot, IBM J. Res. Dev. **7**, 224 (1963).
- [21] S. Kogan, *Electronic Noise and Fluctuations in Solids* (Cambridge Univrsity Press, Cambridge, 1996).
- [22] P. G. Collins, M. S. Fuhrer, and A. Zettl, Appl. Phys. Lett. **76**, 894 (2000).
- [23] L. B. Kiss, U. Klein, C. M. Muirhead, J. Smithyman, and Z. Gingl, Solid State Commun. **101**, 51 (1997).
- [24] D. Sornette, *Critical Phenomena in the Natural Sciences: Chaos, Fractals, Selforganization, and Disorder: Concepts and Tools* (Springer-Verlag, Berlin, 2000).
- [25] A. V. Yakimov and F. N. Hooge, Physica B-condensed matter **291**, 97 (2000).
- [26] P. Varotsos and K. Alexopoulos, Tectonophysics **110**, 73 (1984).
- [27] P. Varotsos, K. Alexopoulos, K. Nomicos, and M. Lazaridou, Nature (London) **322**, 120 (1986).
- [28] P. Varotsos, K. Alexopoulos, K. Nomicos, and M. Lazaridou, Tectonophysics **152**, 193 (1988).
- [29] P. Varotsos and M. Lazaridou, Tectonophysics **188**, 321

- (1991).
- [30] P. Varotsos, K. Alexopoulos, and M. Lazaridou, *Tectonophysics* **224**, 1 (1993).
- [31] P. V. Varotsos, N. V. Sarlis, and M. S. Lazaridou, *Phys. Rev. B* **59**, 24 (1999).
- [32] N. Sarlis, M. Lazaridou, P. Kaporis, and P. Varotsos, *Geophys. Res. Lett.* **26**, 3245 (1999).
- [33] P. Varotsos, N. Sarlis, and M. Lazaridou, *Acta Geophys. Pol.* **48**, 141 (2000).
- [34] P. Varotsos, N. Sarlis, and E. Skordas, *Acta Geophys. Pol.* **48**, 263 (2000).
- [35] P. Varotsos and K. Alexopoulos, *Thermodynamics of Point Defects and their Relation with Bulk Properties* (North Holland, Amsterdam, 1986).
- [36] P. Varotsos, *The Physics of Seismic Electric Signals* (TERRAPUB, Tokyo, 2005).
- [37] P. Varotsos, N. Sarlis, and E. Skordas, *Proc. Jpn. Acad., Ser. B: Phys. Biol. Sci.* **77**, 87 (2001).
- [38] P. Varotsos, N. Sarlis, and E. Skordas, *Proc. Jpn. Acad., Ser. B: Phys. Biol. Sci.* **77**, 93 (2001).
- [39] P. A. Varotsos, N. V. Sarlis, and E. S. Skordas, *Phys. Rev. Lett.* **91**, 148501 (2003).
- [40] P. A. Varotsos, N. V. Sarlis, and E. S. Skordas, *Phys. Rev. E* **66**, 011902 (2002).
- [41] A. Weron, K. Burnecki, S. Mercik, and K. Weron, *Phys. Rev. E* **71**, 016113 (2005).
- [42] P. Bak, C. Tang, and K. Wiesenfeld, *Phys. Rev. Lett.* **59**, 381 (1987).
- [43] P. Bak, *How Nature Works* (Copernicus, New York, 1996).
- [44] T. Antal, M. Droz, G. Györgyi, and Z. Rácz, *Phys. Rev. Lett.* **87**, 240601 (2001).
- [45] J. Davidsen and H. G. Schuster, *Phys. Rev. E* **65**, 026120 (2002).
- [46] K. Hu, P. C. Ivanov, Z. Chen, P. Carpena, and H. E. Stanley, *Phys. Rev. E* **64**, 011114 (2001).
- [47] M. Gardner, *Scientific American* **238**(4), 16 (1978).
- [48] P. A. Varotsos, N. V. Sarlis, and E. S. Skordas (2007), cond-mat/07113766v1.
- [49] P. A. Varotsos, N. V. Sarlis, and E. S. Skordas, *Practica of Athens Academy* **76**, 294 (2001).
- [50] P. A. Varotsos, N. V. Sarlis, and E. S. Skordas, *Acta Geophys. Pol.* **50**, 337 (2002).
- [51] P. A. Varotsos, N. V. Sarlis, and E. S. Skordas, *Phys. Rev. E* **67**, 021109 (2003).
- [52] P. A. Varotsos, N. V. Sarlis, and E. S. Skordas, *Phys. Rev. E* **68**, 031106 (2003).
- [53] P. A. Varotsos, N. V. Sarlis, E. S. Skordas, and M. S. Lazaridou, *Phys. Rev. E* **70**, 011106 (2004).
- [54] P. A. Varotsos, N. V. Sarlis, E. S. Skordas, and M. S. Lazaridou, *Phys. Rev. E* **71**, 011110 (2005).
- [55] P. A. Varotsos, N. V. Sarlis, H. K. Tanaka, and E. S. Skordas, *Phys. Rev. E* **71**, 032102 (2005).
- [56] P. A. Varotsos, N. V. Sarlis, H. K. Tanaka, and E. S. Skordas, *Phys. Rev. E* **72**, 041103 (2005).
- [57] N. V. Sarlis, P. A. Varotsos, and E. S. Skordas, *Phys. Rev. B* **73**, 054504 (2006).
- [58] P. A. Varotsos, N. V. Sarlis, E. S. Skordas, H. K. Tanaka, and M. S. Lazaridou, *Phys. Rev. E* **73**, 031114 (2006).
- [59] P. A. Varotsos, N. V. Sarlis, E. S. Skordas, H. K. Tanaka, and M. S. Lazaridou, *Phys. Rev. E* **74**, 021123 (2006).
- [60] P. A. Varotsos, N. V. Sarlis, E. S. Skordas, and M. S. Lazaridou, *Appl. Phys. Lett.* **91**, 064106 (2007).
- [61] S. Abe, N. V. Sarlis, E. S. Skordas, H. K. Tanaka, and P. A. Varotsos, *Phys. Rev. Lett.* **94**, 170601 (2005).
- [62] B. Lesche, *J. Stat. Phys.* **27**, 419 (1982).
- [63] B. Lesche, *Phys. Rev. E* **70**, 017102 (2004).
- [64] U. Tirnakli and S. Abe, *Phys. Rev. E* **70**, 056120 (2004).
- [65] M. Abramowitz and I. Stegun, *Handbook of Mathematical Functions* (Dover, New York, 1970).
- [66] V. K. B. Kota, V. Potbhare, and P. Shenoy, *Phys. Rev. C* **34**, 2330 (1986).
- [67] P. A. Varotsos, N. V. Sarlis, and E. S. Skordas (2007), cond-mat/0703683.

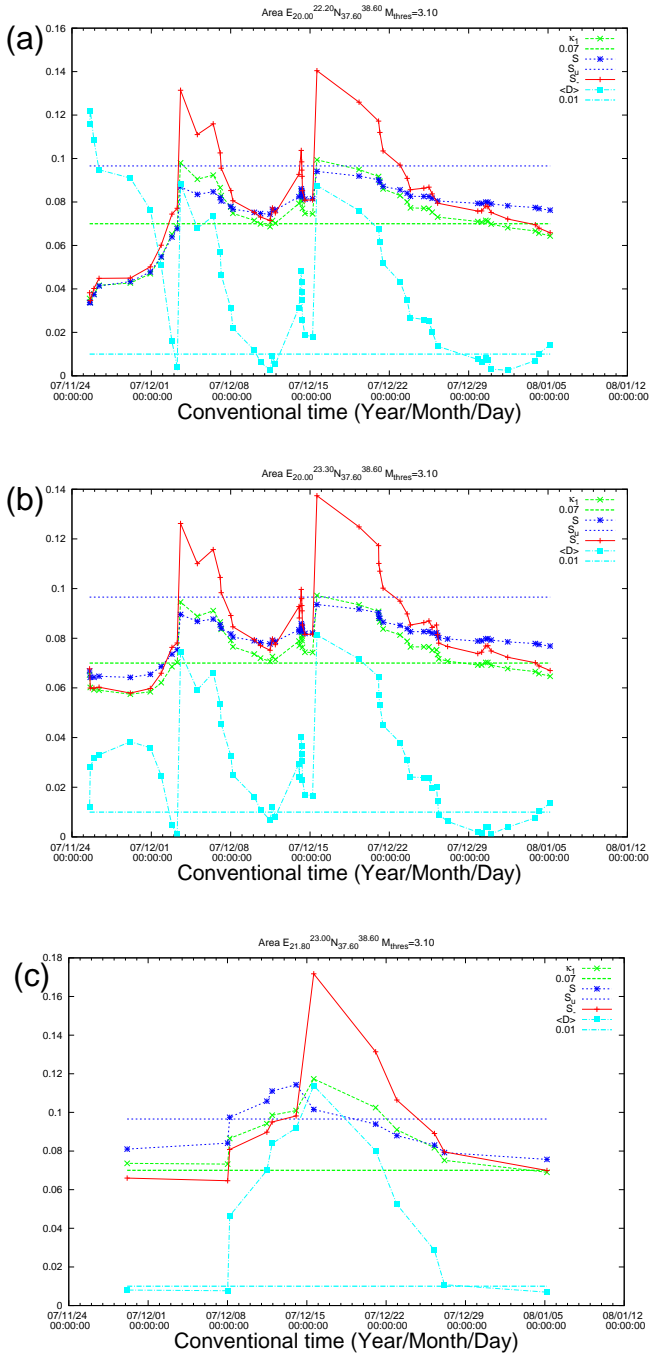


FIG. 14: (color online) The evolution of the parameters  $\langle D \rangle$ ,  $\kappa_1$ ,  $S$  and  $S_-$  for the period: since the submission of the previous version of the present paper until just before the 6.6 earthquake on 6 January, 2008. (a), (b) correspond to the two areas depicted in Fig.13, while (c) to the dark shaded area in Fig.15,  $M_{thres} = 3.1$ .

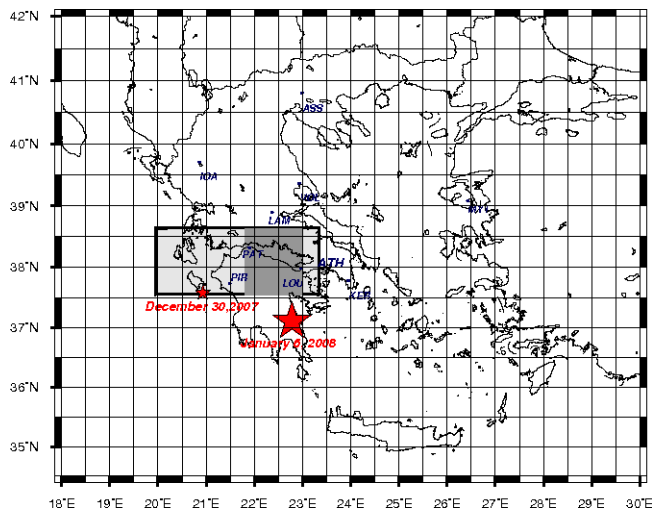


FIG. 15: (color online) The map shows the epicenters of the 5.3 earthquake on 30 December, 2007 (small star) and the 6.6 earthquake on 6 January, 2008 (large star). The dark shaded area depicts the part of the larger area  $N_{37.6}^{38.6} E_{20.0}^{23.3}$  adjacent to the epicenter of the 6.6 earthquake, whose the four parameters  $\langle D \rangle$ ,  $\kappa_1$ ,  $S$  and  $S_-$  fulfilled the conditions for a true coincidence just one day before the major earthquake occurrence (see Fig.14(c)).

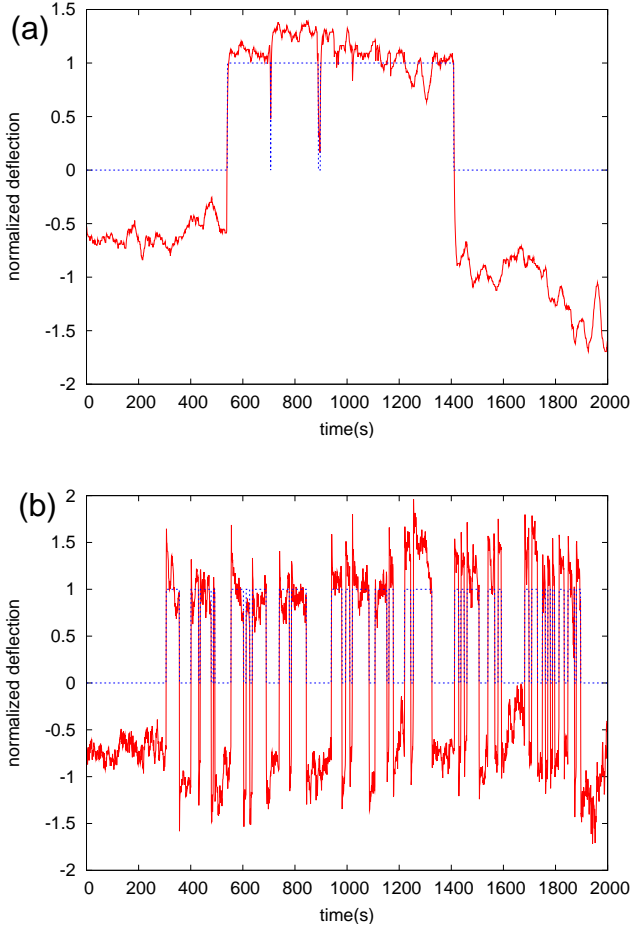


FIG. 16: (color online) The electric signals recorded on 10 January, 2008 at PAT (a) and on 14 January, 2008 at PIR (b), in a fashion similar to that of Fig.6(a)

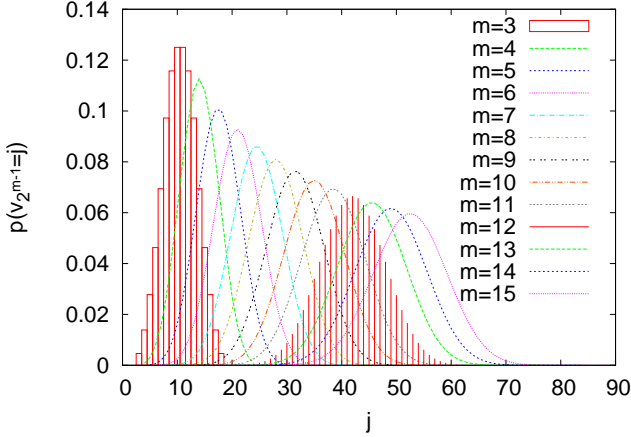


FIG. 17: (color online) The probabilities  $p(v_{2^{m-1}} = j)$  as a function of  $j$  for various  $m$ . They are clearly skewnessless, i.e., symmetric around their median. Here, as in Ref.[47], 6-sided dices ( $k = 6$ ) were considered. For the reader's convenience  $p(v_{2^{m-1}} = j)$  for  $m = 3$  and  $m = 12$  have been drawn with a different style.